*Desalination and Water Treatment*
www.deswater.com

doi:10.5004/dwt.2019.23883

148 (2019) 312–323
April

# Comparison of zero valent iron and zinc oxide green nanoparticles loaded on activated carbon for efficient removal of Methylene blue

Mohammad Reza Miri[a], Rasoul Khosravi[b,*], Ali Akbar Taghizadeh[b], Mehdi Fazlzadehdavil[c,d], Zahra Samadi[b], Hadi Eslami[e], Abdollah Gholami[f], Esmaeil Ghahramani[g]

[a]*Social Determinants of Health Research Center, Department of Health Education and Health Promotion, School of Health, Birjand University of Medical Sciences, Birjand, Iran, email: miri_moh2516@yahoo.com (M.R. Miri)*
[b]*Social Determinants of Health Research Center, Department of Environmental Health Engineering, School of Health, Birjand University of Medical Sciences, Birjand, Iran, email: Khosravi.r89@gmail.com (R. Khosravi), aliakbar.taghizadeh@gmail.com (A.A. Taghizadeh), samadi.zahra14@yahoo.com (Z. Samadi)*
[c]*Social Determinants of Health Research Center, Ardabil University of Medical Sciences, Ardabil, Iran*
[d]*Department of Environmental Health Engineering, School of Public Health, Tehran University of Medical Sciences, Tehran, Iran, email: m.fazlzadeh@gmail.com (M. Fazlzadehdavil)*
[e]*Occupational Environment Research Center, Department of Environmental Health Engineering, School of Health, Rafsanjan University of Medical Sciences, Rafsanjan, Iran, email: hadieslami1986@yahoo.com (H. Eslami)*
[f]*Social Determinants of Health Research Center, Department of Occupational Health Engineering, School of Health, Birjand University of Medical Sciences, Birjand, Iran, email: gholamiabdollah@yahoo.com (A. Gholami)*
[g]*Environmental Health Research Center, Research Institute for Health Department, Kurdistan University of Medical Sciences, Sanandaj, Iran & phD student of Environmental Health Engineering, School of public Health, Hamadan UNiversity of Medical Sciences, Hamadan, Iran, email: ghahramani64@gmail.com (E. Ghahramani)*

Received 26 December 2017; Accepted 29 January 2019

**ABSTRACT**

In this study, iron nanoparticles (GnZVI) and zinc oxide nanoparticles (GnZnO) were synthesized by *Peganum harmala* seeds extract using green method, and were loaded on activated carbon derived from *P. harmala* seed (AC). TEM analysis showed that the nanoparticle size was smaller than 100 nm, while EDAX analysis confirmed that GnZVI and GnZnO were stabilized on AC. BET analysis showed that GnZnO/AC and GnZVI/AC special surface areas were 208 and 107 $m^2/g$, respectively. Moreover, the FTIR analysis showed the role of polyphenolic groups in the synthesis of nanoparticles. It was generally found that GnZnO/AC showed higher efficiency in the adsorption of methylene blue as compared with GnZVI/AC.

*Keywords:* Activated carbon; Adsorption; Green synthesis; Methylene blue; nZVI

## 1. Introduction

The rapid population growth and urbanization has resulted in the deterioration of many water resources around the world [1–3]. Many chemicals are extensively used in numerous industries [4]. Among them, dyes and organic compounds are vastly used in industry and every-day life [5–7]. The annual production rate of commercial dyes and dyeing materials has been estimated to be higher than 100000 and 700000 tons, respectively [8–10]. Dyeing materials are applied in various industries such as textile, leather, paper, plastic etc [11,12]. The discharge of dye containing effluents from these industries creates serious problems such as increased toxins and COD, reduced light penetration and disruption of photosynthesis process [5,13,14]. Moreover, dyes bring about allergy, dermatitis, skin irritation, cancer and genetic mutations in humans [15,16]. Methylene blue is used as base color in dye-

*Corresponding author.

ing paper, wool and cotton [17,18]. Inhalation of methylene blue would impair respiration, and direct exposure to it may cause permanent damages to the eyes of humans and animals, local burns, nausea and vomiting, increased sweating, mental disorders and methemoglobinemia [8,9,19]. Today, a variety of technologies have been developed specially to remove organic materials from sewages. Some of these methods include chemical coagulation, electrocoagulation, ion exchange, membrane filters, adsorption, ozonation, Fenton, photo-Fenton and other chemical oxidation processes [9,15,19–26]. Adsorption is a physical process [13,27] with broad application, which has attracted the attention of many researchers [28,29]. It also has advantages in wastewater treatment such as high efficiency and ease of use [17,30,31]. Until recently, activated carbon has been widely used to remove organic colors, but it also has limitations such as high cost of production and purification [13,32], low adsorption capacity [17,33] and limited degradability [34]. Significant efforts have been made to select a suitable replacement, with high adsorption capacity, low cost and ability to rapidly remove color [8,35]. Nanoparticles with high surface to volume ratio [36,37], in addition to metal and metalloid behavior, possess significant properties including large number of active atoms and existence of empty active sites on the surface of the adsorbent. As a result, in order to overcome the limitations of activated carbon and increased rate of adsorption, the structure of the nanomaterial should be loaded on the surface of the activated carbon. The use of materials such as zinc oxide nanoparticles as a strong adsorbent on other adsorbents (e.g. activated carbon) has certain advantages. This process could increase the number of active adsorption sites inside the adsorbent and solve the problems related to the separation of nanoparticles from solution [38,39]. It can also significantly increase the percentage of contaminants removal by increasing the adsorption capacity and number of active adsorbent atoms [17]. Effective techniques have been applied for synthesis of nanoparticles such as sol-gel, thermal decomposition, hydrothermal synthesis, as well as spray pyrolysis methods [5,40]. The green synthesis of nanoparticles is preferred to other known methods because it is economical and environmentally friendly [41–43] fazlz *Peganum harmala* is a wild plant that grows in *Central Asia*, *Middle East*, and *Africa* and it's seeds have active alkaloids called harmine and harmaline that is useful for many proposes [44,45]. Considering the above mentioned facts, we have used from *P. harmala* seed as precursor for activated carbon and nanoparticles preparation in this study. And then we investigate a comparative evaluation of methylene blue removal from aqueous solutions with activated carbon loaded with iron and zinc oxide nanoparticles produced by green synthesis method.

## 2. Materials and methods

### 2.1. Preparation of activated carbon

*Peganum harmala* seeds were collected from their pods and from the surrounding areas of *Birjand* city, Iran. They were held under sunlight for three days after being isolated and cleaned so that the moisture can be completely removed. The granular pellets were then powdered using a mill. The powders were isolated by mesh 60, completely soaked in 50% phosphoric acid and kept at ambient temperature for 48 h. Subsequently, they were transferred into a cylindrical-shaped steel reactor with lid. The steel reactor was moved inside an adjustable HL40P furnace, its temperature reached 500°C at 5 rpm and remained at this temperature for 2 h. After cooling the furnace, the reactor was removed and for activation, the resulted carbon powder was immersed into normal hydrochloric acid (3%) inside a 500 ml beaker. Thereafter, it was transferred into *Elmasonic E 20H* ultrasonic with 37 KHz frequency and was kept for one hour. The resulting activated carbon was washed with distilled water twice, so that its pH reaches above 6. The powdered activated carbon was placed in an oven for 2 h at 110°C until it was completely dry. Carbon was stored in a container away from moisture for further use.

### 2.2. Green synthesis of nanoparticles

An extract of the raw powder of *P. harmala* seed was used to implement synthesis using the green method. In the present study, 6 g of *P. harmala* powder was poured into 500 ml *Erlenmeyer* flasks and 100 ml of distilled water was added and then placed on a magnetic stirrer. The stirrer's speed was set at 300 rpm for mixing, and the temperature of the solution was controlled at 80°C. After one hour of the extraction process, the solution was taken from the heating magnetic stirrer and filtered using a vacuum pump after being cooled. The extract, which comprised zinc nitrate or ferric chloride of 0.1 M was mixed in a ratio of 4 to 1. Afterward, the solution was transferred into an ultrasonic bath and allowed to stay for one hour. The synthesis of zinc oxide nanoparticles was detected with a white clot and that of iron nanoparticles with a brown-black color clot. After the ultrasonic time, the mixture was poured into a measuring cylinder, washed with ethanol three times and then rinsed with distilled water again. The remaining mixture was transferred into an oven at 50°C until it was completely dry. After drying the nanoparticles, it was powdered with mortar and stored for further use.

### 2.3. Loading nanoparticles on activated carbon

After the production of activated carbon and nanoparticles synthesis, 0.05 g of nanoparticles was poured in 200 ml of distilled water and was placed on a magnetic stirrer for 10 min in order to obtain a homogenous solution. Thereafter, 5 g of activated carbon was added to the solution and placed on a magnetic stirrer at 500 rpm for 10 h in order to load the nanoparticles on AC. The adsorbents were then isolated with filter papers and rinsed with double distilled water. It was then completely dried in an oven at 95°C for 10 h, and nanoparticles stabilization was conducted on AC. The adsorbents were kept in polyethylene containers away from moisture.

### 2.4. Materials and adsorption tests

This is an experimental batch study implemented in 100 cc *Erlenmeyer flasks* on shaker. To prepare different concentrations of methylene blue, 1000 mg/l methylene blue stock solution was used. To conduct the experiments, 50 cc of samples with defined concentration was removed using graduated cylinders and poured into an *Erlenmeyer flask*. In cases where pH adjustment was necessary, the desirable

pH solution was prepared using HCI and NaOH. Then a definite dose of adsorbent was measured and added to the sample in the *Erlenmeyer flask*. It was immediately placed on a shaker and the stirrer speed was adjusted. After the intended contact time, the samples were removed from the shaker and passed through 0.45 micron *Whatman filter paper*. The filtered samples were used for evaluation of the remaining amount of dye. The most important variables in the experiment included initial pH solution with 2–12 range, 0.5–6 g/L adsorbent dose, 2–80 min contact time, 25–300 mg/L initial concentration of dye and 0–300 rpm stirring speed. To ensure repeatable results, each step of the experiment was repeated twice and the average results were reported. All materials used were of analytical grade and were the products of *Merck Company*.

### 2.5. Characterization of adsorbents

To determine the size of the produced nanoparticles the nanoparticle samples were dispersed in methanol for 20 min and a drop of it was spilled on grid and placed in the Philips CM30 transmission electronic microscope (TEM; 120 KeV). To evaluate the morphology of the nanoparticles and AC loaded with nanoparticles, the FESEM analysis was applied. EDAX analysis was also used to confirm the loading of nanoparticles on AC. These analyses were conducted using FESEM/EDAX machine, *Mira3-XMU* model. The specific surface area and pore structure of adsorbents was measured by N2 (–250°C) adsorption using *Belsorp mini II* (*Bel Japanese Comp*any). The surface area and pore size distribution were determines using *Brunauer–Emmett–Teller* (BET) method. To identify the functional groups on the adsorbent, Fourier transform infrared spectroscopy (FTIR) was conducted using *Spectrum RXI (PerkinElmer; US)*. Analysis of samples: The present study used a colorimetric method by *UV/VIS Spectrometer T80+*, at a wavelength of 665 nm, for the measurement of color [46]. Data were analyzed using *Excel* software.

The amount of MB adsorbed onto adsorbents, $q_e$ (mg g$^{-1}$) was calculated as follows:

$$q_e = \frac{(C_0 - C_t) \times V}{m} \tag{1}$$

where $C_0$ (mg/l) and $C_t$ (mg/l) are the initial and equilibrium concentration of MB, respectively. $q_e$ (mg/l) is amount of MB adsorbed, $M$ (g) is the mass of the adsorbent and $V$ (l) is the volume of the liquid phase.

Also the removal percentage (R%) of MB was calculated for each run by using Eq. (2) [47] Q:

$$R(\%) = \left(1 - \frac{C_t}{C_0}\right) \times 100 \tag{2}$$

where $C_0$ and $C_t$ (mg/l) were the initial and final concentration of MB in the solution, respectively.

## 3. Results and discussion

### 3.1. Adsorbent characterization

The TEM images related to GnZnO and GnZVI are respectively shown in Figs. 1a and b. These images confirmed the synthesis of nano-sized particles and showed that the size of the produced nanoparticles is smaller than 100 nm. The comparison of zinc oxide and iron nanoparticles shows that the size of GnZnO was smaller than GnZVI, and GnZnO had an almost spherical shape, however it was seen as multifaceted. The produced nanoparticles had one shell, indicating that stabilization factors in *P. harmala* seeds extract are wrapped around the core. EDAX analysis, in addition to qualitative status, also defines the quality of elements. Fig. 2 demonstrates the elements present on AC. There is neither iron nor zinc in this figure. Figs. 2b and 2c respectively show the profile of GnZVI/AC and GnZnO/AC elements. As shown in this figures, it is clear that iron and zinc are apparent on AC. This analysis confirms the stabilization of nanoparticles on AC surface. The FESEM analysis was used to examine the morphological properties, as well as the status of nanoparticles loaded on activated carbon. For this purpose, several images with 200 kx zoom were prepared for nanoparticle and 100 kx zoom for activated carbon loaded with nanoparticles. Fig. 3a and 3b respectively show images of the GnZVI and GnZVI/

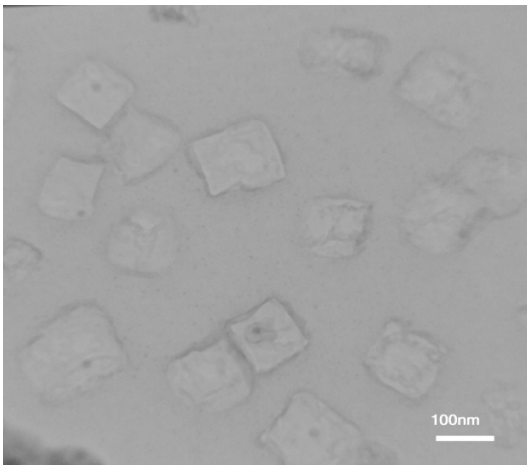


(a)

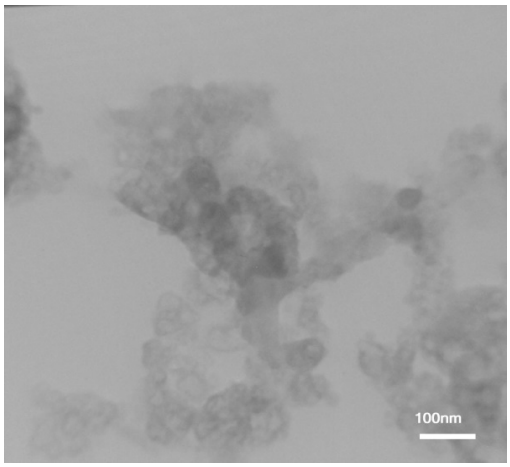


(b)

Fig. 1. TEM images of the GnZVI (a) and GnZnO (b).

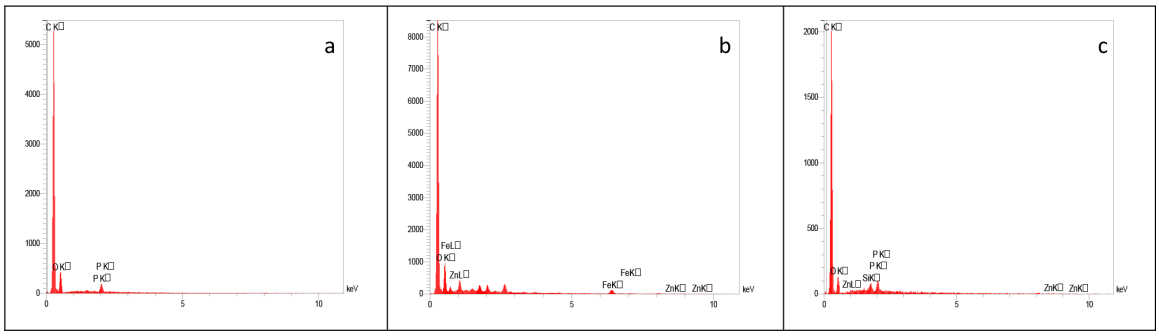


Fig. 2. EDAX analysis of the AC (a), GnZVI/AC (b), and GnZnO/AC (c).

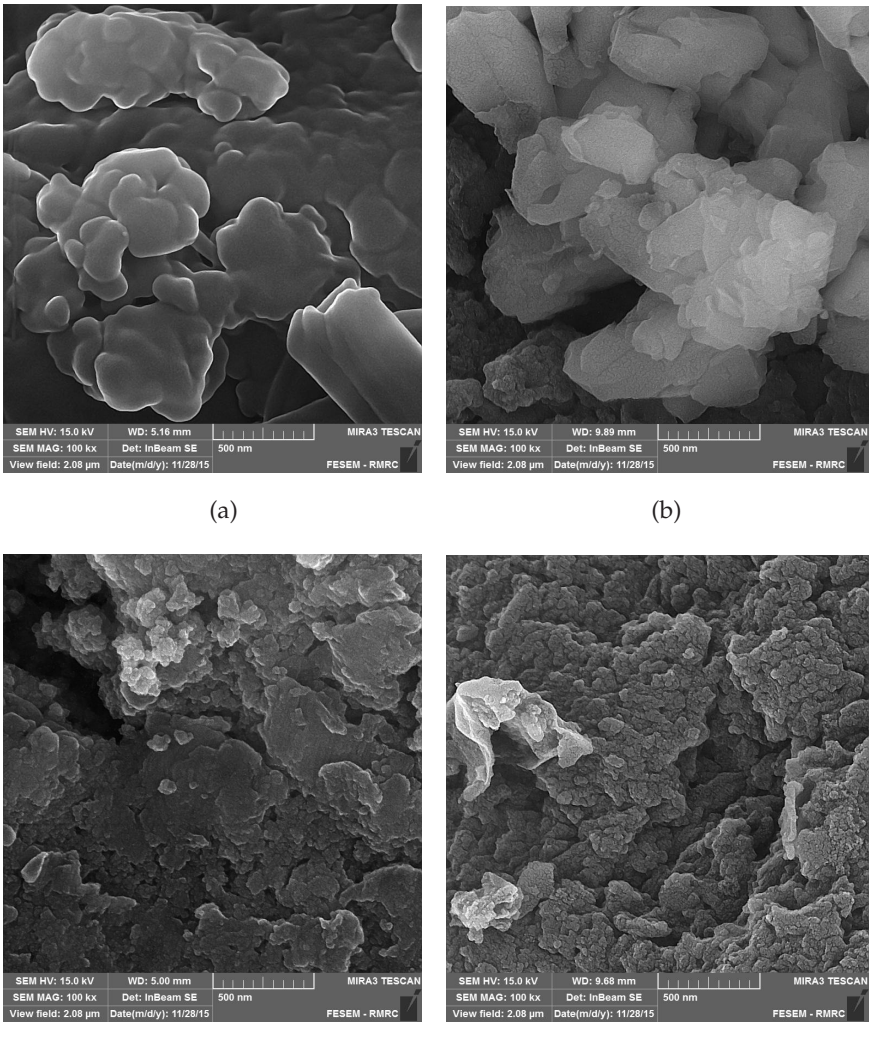


Fig. 3. FESEM images of the GnZVI (a), GnZVI/AC (b), GnZnO (c), and GnZnO/AC (d).

AC surface. Fig. 3c and 3d respectively show images of the GnZnO and GnZnO/AC. In these images, similar to TEM, the zinc nanoparticles are much smaller than iron, while more agglomeration is visible in GnZVI. This caused the loading of iron nanoparticles on AC not to be evenly and uniformly conducted, as shown in Fig. 3b. This figure shows that GnZVI accumulation on the surface of activated carbon would reduce the surface area of adsorbent and improve the function of adsorbents. The zinc nanoparticles were stabilized on AC in smaller size and with higher uniformity. Thus, this could improve the adsorbent function in the process of removal. BET analysis also confirmed

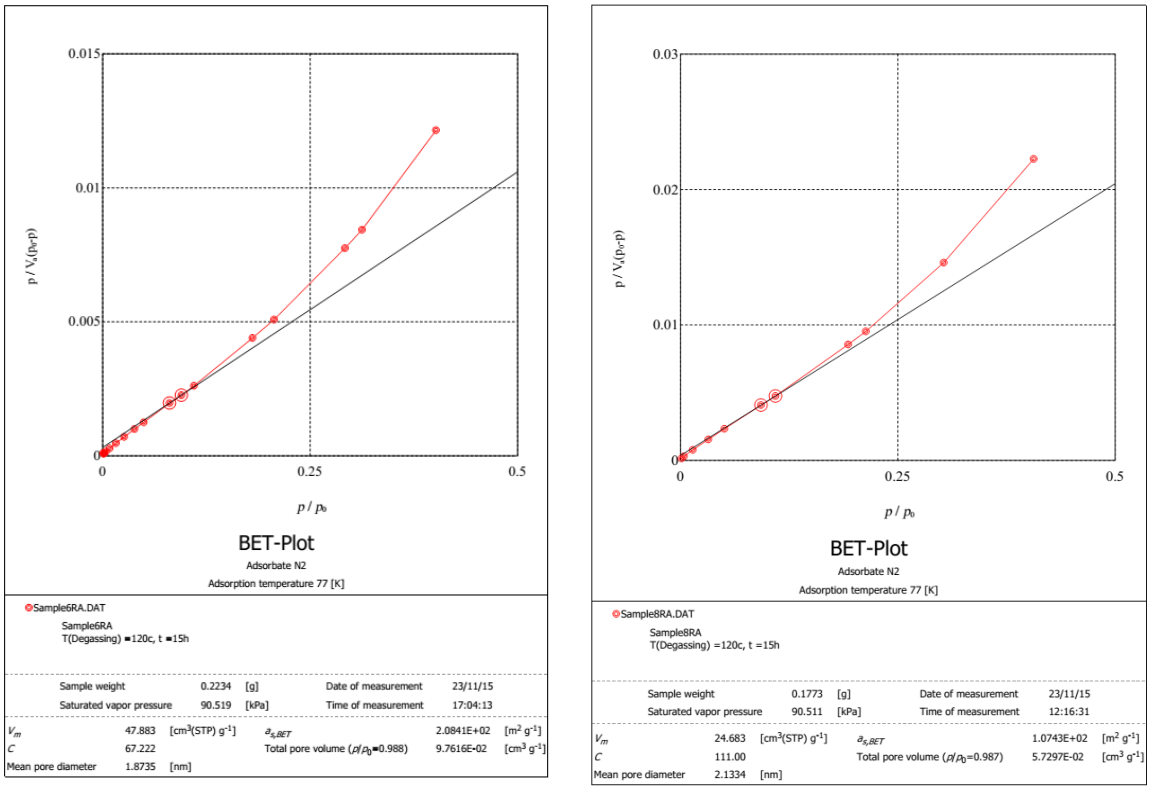


(a) (b)

Fig. 4. BET plots of GnZnO/AC (a) and GnZVI/AC(b).

the results of FESEM analysis. BET analysis was applied to determine the surface area, mean pore diameter, as well as total volume of adsorbent pores. As shown in Fig. 4, the total volume of pores in activated carbon loaded with zinc oxide and iron nanoparticles were $9.76 \times 10^{-2}$ and $5.73 \times 10^{-2}$ $cm^3/g$, respectively. The mean pore diameter for GnZnO/AC and GnZVI/AC were equal to 1.87 and 2.13 nm, respectively. The specific surface area of GnZnO/AC and GnZVI/AC were respectively 208 and 107 $m^2/g$. The analysis indicated that the special area of GnZnO/AC was almost double that of GnZVI and as such, possess more accessible area for contact between the adsorbent and absorbed material. Overall the surface area of both adsorbents was relatively high. Therefore, large area and porous structure increased the transfer of pollutants toward adsorbents [48].

FTIR analysis was conducted on GnZnO (Fig. 5a) and GnZVI (Fig. 5b) to identify the interaction between biomolecules of *P. harmala* seeds extract and metal ions, which are responsible for formation and stabilization of nanoparticles.

A very intense and broad band appeared in region 3500–3200 $cm^{-1}$ on both nanoparticles. Absorption in this region indicated O-H stretch of the hydroxyl functional groups of alcoholic and phenolic compounds. Although the mechanism of formation of nanoparticles using synthesis is still not clear, but in general, it has been shown that the presence of phenolic compounds causes the reduction of nanoparticles [49–51]. It is evident that the most effective functional groups involved in the production of nanoparticles hold the strongest and widest peak on both nanoparticles. These peaks show the dominance of phenolic groups in FTIR spectrum for both nanoparticles. The presence of conjugated double bonds accompanied with abundant phenolic –OH groups provide a favorable molecular configuration for the effective delocalization of the unpaired electron and this can be attributed to the free radical scavenging potential of the *P. harmala* seed-extracts. It has been documented that the antiradical activity of any molecule is stoichiometric with the concentration of phenolic OH groups, and a positive correlation exists between the antioxidant activity and the abundance of OH group of the phenolic moiety [52].

### 3.2. *Effect of pH*

The results of tests to determine the optimum pH is given in Fig. 6a. Accordingly, in 100 mg/l concentration, methylene blue color and amount of 2 g/l adsorbent along with increased pH from 2 to 12 for nanoGnZVI/AC, increased the efficiency of methylene blue removal from 22.69 to 77.61%, while for nanoGnZnO/AC, it increased from 43.68 to 97.04%. Previous studies have shown that the pH of the solution could affect the adsorbent surface load, degree of ionization in different pollutants, separation of functional groups on adsorbent active sites and dye molecule structure [54]. Solution pH could affect environmental chemistry and adsorbent surface bonding and as such, it is an extremely important parameter in the process of adsorption. Methylene blue is acationic dye existing in aqueous environments as positive ions [55]. Increased

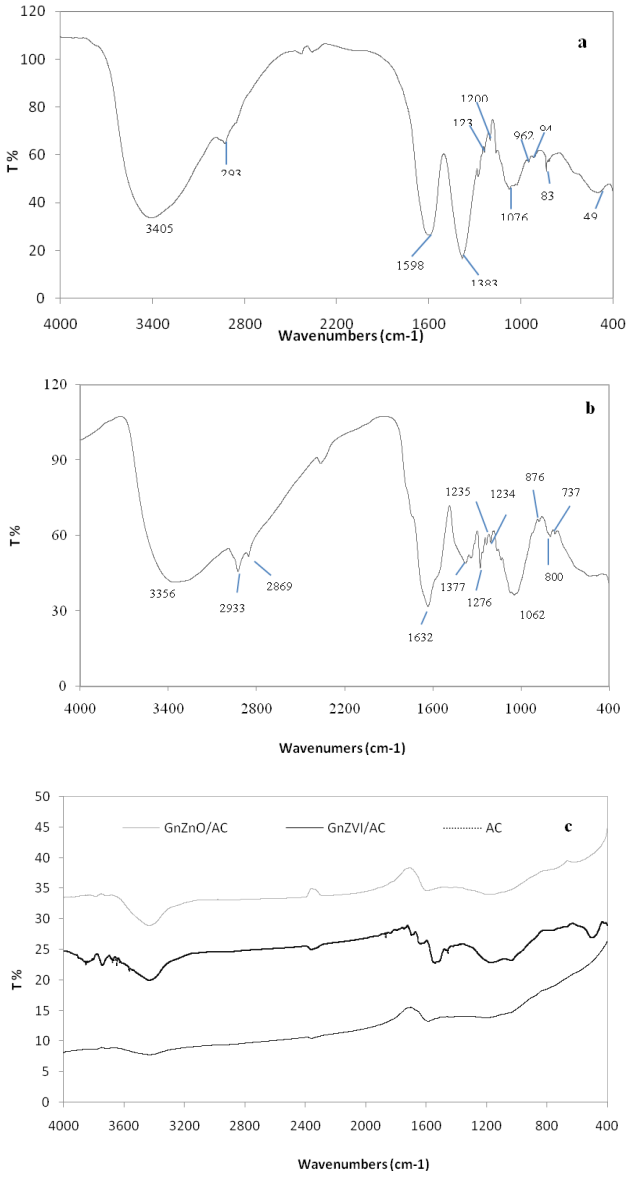


Fig. 5. FTIR spectrum of the GnZnO (a), GnZVI (b), AC, GnZnO/AC and GnZVI/AC (c).

adsorption along with increased amount of hydroxide in the environment is as a result of change in the adsorbent surface charge and the level of ionization of methylene blue present in solution. On the other hand, the cationic molecule of methylene blue possesses agent groups of S and H ionized in water, which cause the molecule to be cationic and therefore, the negative charges of the adsorbent surface (adsorbents PHzpc are equal to 6.2) adsorb the cationic ions of methylene blue [56]. The changes in the removal efficiency is noticeable when the pH of the solution is higher than 8. In fact, the high pH along with increased negative charge of adsorbent area leads to improvement of electro statistic forces of positive ions of cationic dye [19] and help the binding of adsorbent with MB dye cations by two type of interactions (electrostatic interaction as well as hydrogen bonding) [57]. On the other hand, it is evident that the adsorption of methylene blue dye decreases in acidic pH and this decrease of adsorption in acidic environments may be due to the presence of excessive $H^+$ and protonation of adsorbent active sites [58] which compete with cationic dye to be adsorbed on the adsorbent sites [55]. This finding is consistent with the studies of Moussavi et al. [46] and Jain et al. [19].

### 3.3. Effect of adsorbent dosage

Fig. 6b shows that by increasing the amount of adsorbent dosage from 0.5 to 6 g/l, the efficiency removal of methylene blue increases. Besides, by increasing GnZVI/AC and GnZnO/AC from 0.5 to 6 g/l, the dye removal efficiency increased from 44.72 to 94.4% and from 53.20 to 99.81% respectively. In fact, the increased removal rate by dosage increasing is the consequence of more active and accessible adsorbent sites and their broader surface. The figure also shows that by increasing the adsorbent dosage, the adsorption capacity for both adsorbents decreased, though as the GnZnO/AC dose increased from 0.5 to 6 g/l, the adsorption capacity decreased from 110.4 to 17.26 mg/g. It also decreased from 92.8 to 16.32 mg/g in the GnZVI/AC adsorbent. This result indicated that the adsorbed dyes may either block access to the internal pores or cause particles to aggregate, thereby resulting in unavailability of active sites for adsorption [59,60]. The findings of the present study are consistent with other studies [15,46,59].

The findings of this study also showed that the removal efficiency of dye using GnZnO/AC nanoparticles was much better than GnZVI/AC. This fact was less noticeable in smaller dosages and is economically more significant because smaller adsorbent dosages could render more desirable results.

### 3.4. Effect of contact time

Contact time as one of the effective parameters was applied to define the optimal performance of adsorption. As shown in Fig. 6c, the amount of removed dye increased due to longer contact time, and the remaining dye in the solution decreased. The removal efficiency at 2 min contact time for GnZnO/AC and GnZVI/AC were 82.8 and 74.3%, respectively. The removal efficiency increased to 98.83% after 15 min for GnZnO/AC and increased for GnZVI/AC to 98.68% after 40 min. After the time was specified for each adsorbent, the efficiency did not change, therefore, it could be considered as the equilibrium removal time. However, after this time, the amount of removed dye did not change and as such, it can be defined as the equilibrium removal time which signifies the saturation time. The maximum amount of dye removed at the equilibrium time is called the equilibrium adsorption capacity [15]. The dye removal process occurs very quickly and this may be due to the absence of internal diffusion resistance. It is expected that the external resistance to mass transfer is negligible in aqueous solution which is a reasonable condition in adsorption systems with proper mixing. In addition, shorter contact time in adsorption system will reduce the capital and operational costs to a full-scale application [13]. Fig. 6c shows that the equilibrium time for GnZnO/AC adsorbent is shorter than

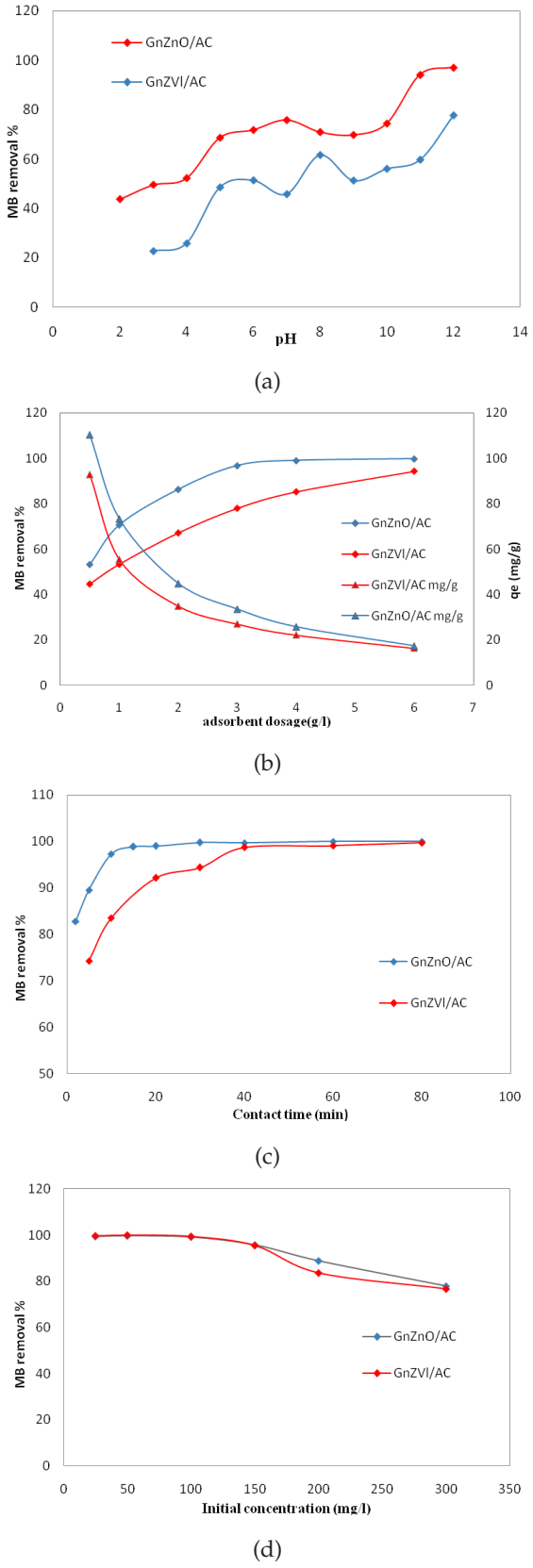


Fig. 6. Influence of initial pH (a), adsorbent dosage (b), contact time (c) and initial dye concentration (d) on MB removal by adsorbents.

the GnZVI/AC adsorbent. Also, it shows the high efficiency of GnZnO nanoparticles in the removal process.

### 3.5. Effect of initial dye concentration

Fig. 6d demonstrates the effect of initial dye concentration of methylene blue on the two adsorbents, GnZVI/AC and GnZnO/AC. The figure shows that, in GnZnO/AC adsorbent, the increased initial concentration of methylene blue from 25 to 300 mg/l at 15 min contact time caused the removal efficiency to decrease from 99.34 to 77.89%. The increased initial concentration of methylene blue from 25 to 300 mg/l at 40 min contact time in the GnZVI/AC adsorbent decreased the removal efficiency from 99.62 to 76.63%. The reduced percentage of methylene blue with increased concentration could be justified in a way that since the adsorbent mass for all concentrations is stable, methylene blue molecules must compete for locations with higher probability of adsorption. Notably, the removal percentage decrease with increase in initial dye concentration [46]. On the other hand, increased adsorption capacity occurred due to the propulsion provided by the concentration to overcome the resistance of dye mass transfer between aquatic and solid phases. Therefore, a higher initial concentration of the dye increases the adsorption capacity [61].

### 3.6. Adsorption kinetics

Methylene blue adsorption rate on the adsorbent solution quality is a significant factor to control water quality. For this purpose, laboratory data of first-order and pseudo-second-order kinetic were used to determine the kinetics followed by the adsorption process.

The linear form of first order kinetic model is as Eq. (3):

$$\ln\left(q_{eq}-q\right)=\ln q_{eq}-\frac{K_1 t}{2.303} \tag{3}$$

where $q_{eq}$ (mg/g) is the amount of methylene blue adsorbed per gram of adsorbent at equilibrium time, $q$ is the amount of methylene blue adsorbed per gram of adsorbent at time t, and $k_1$ is the first-order kinetic constant ($min^{-1}$) which is calculated by $\ln\left(q_{eq}-q\right)$ chart slope versus $t$.

The linear form of second-order kinetic model is expressed as Eq. (4) [62]:

$$\frac{t}{q}=\frac{1}{K_2 q_{eq}^2}+\frac{1}{q_{eq}}t \tag{4}$$

The $\frac{t}{q}$ chart in proportion to $t$ is a straight line, with $\frac{1}{q_{eq}}$ slope and $\frac{1}{K_2 q_{eq}^2}$ intercept. Accordingly, $q_{eq}$ and $K_2$ values are respectively calculated according to slope and intercept [63].

$k_2$ is the second-order kinetic constant (g/mg·min) which is the intersection point of $\frac{t}{q_{eq}}$ chart vs. $t$.

According to the results presented in Table 1 and Figs. 7a and 7b, it can be concluded that the pseudo second-order $R^2$ kinetic for both adsorbents shows that the adsorption behav-

Table 1
Kinetic parameters for pseudo-first order and pseudo-second order

| Adsorbents | Pseudo-first order | | | Pseudo-second order | | |
|---|---|---|---|---|---|---|
| | $q_e$ | $K_1$ | $R^2$ | $q_e$ | $K_2$ | $R^2$ |
| GnZnO/AC | 4.72 | 0.293 | 0.947 | 33.55 | 0.0793 | 0.99998 |
| GnZVI/AC | 10.84 | 0.162 | 0.942 | 34.12 | 0.0138 | 0.99985 |

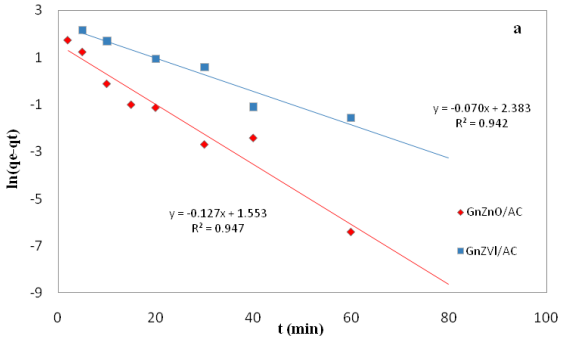


(a)

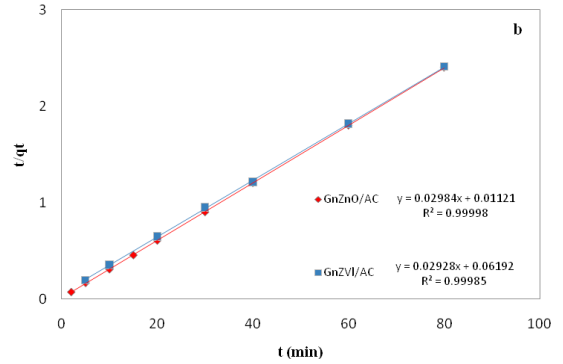


(b)

Fig. 7. Pseudo-first order (a) and Pseudo-second order kinetic (b) plots for the MB adsorption on GnZnO/AC and GnZVI/AC.

ior follows the second-order kinetic. The constant speed of $k_2$ for GnZnO/AC is 7.9 × $10^{-2}$ and 1.38 × $10^{-2}$ for GnZVI/AC, indicating that the methylene blue adsorption speed of GnZnO/AC is 5.7 times more than that of GnZVI/AC.

### 3.7. Adsorption isotherm study

For evaluation of GnZVI/AC and GnZnO/AC performance in the removal of MB, isotherm studies were conducted. Isotherm models are important items for evaluation of an adsorbent behavior. Thus the sorption isotherms were investigated using two models namely Langmuir and Freundlich isotherm models. Langmuir isotherm assumes that the uptake of contaminant on to a solid adsorbent is a monolayer adsorption with a finite number of biding site. Langmuir isotherm is commonly used to monolayer, and the Freundlich isotherm to multilayer adsorption processes on heterogeneous surface and active sites with different energy. Langmuir model in linear form can be expressed as Eq. (5):

$$\text{Langmuir}: \frac{C_e}{q_e} = \frac{1}{K_l \times q_{max}} + \frac{C}{q_{max}} \quad (5)$$

where $C_e$ is final MB concentration (mg/l), $q_e$ is amount of MB adsorbed on adsorbents (mg/l) and $K_l$ (L/mg) is Langmuir constants related to energy of adsorption. The fundamental characteristics of the Langmuir equation can be described in term of the Langmuir dimensionless separation factor, $R_L$ defined as Eq. (6):

$$R_L = \frac{1}{1+\left(q_{max} \times K_L\right)C_0} \quad (6)$$

The $R_L$ values indicate the type of isotherm to be unfavorable ($R_L > 1$), linear ($R_L = 1$), favorable ($0 < R_L < 1$) and irreversible ($R_L = 0$). Linear form of Freundlich isotherm model was used as Eq. (7):

$$\text{Freundlich}: ln\, q_e = ln\, K_f + \frac{1}{n} ln\, C_e \quad (7)$$

where $K_f$ is maximum adsorption capacity (mg/l), and $1/n$ is the constant indicative of the intensity of the adsorption, $n$ values between 1 and 10 represents beneficial adsorption [36].

Fig. 8a shows the plotted models with related regression coefficients. Higher determination coefficients ($R^2$) for Langmuir model in the figure suggest that the adsorption of MB on both adsorbents best fitted with Langmuir model. Thus, it can be concluded that adsorption of MB on GnZVI/AC and GnZnO/AC occurs as a monolayer phase on a homogenous surface [41]. Considering the Langmuir constant, adsorption energy of MB on GnZnO/AC and GnZVI/AC were 0.375 and 0.395 l/mg, respectively. Furthermore, as can be seen in Table 2, the values of $K_f$ and $n$ in Freundlich model were found to be 23.47 and 3.15 for GnZnO/AC and 26.57 and 3.98 for GnZVI/AC, respectively. The $n$ values for both of adsorbents, representing good adsorption potential for both adsorbents and indicates that the MB adsorption is favorable at studied condition [36]. The maximum adsorption capacity of GnZnO/AC and GnZVI/AC for MB were 78.74 and 74.62 mg/g which indicate adsorption capability of GnZnO/AC is higher than GnZVI/AC.

As shown in Fig. 9, the values of RL for GnZVI/AC and GnZnO/AC is between 0.008 and 0.09 since the value of $R_L$ near to 0 in the Langmuir model demonstrates that adsorption of MB on these adsorbents is favorable and irreversible [64].

### 3.8. Adsorption mechanisms

Generally, several factors, such as adsorbent structure, physico-chemical properties of adsorbent, and interaction

Table 2
Isotherm constant for MB adsorption on GnZVI/AC and GnZnO/AC

| Langmuir | | | | Freundlich | | |
|---|---|---|---|---|---|---|
| | $q_{max}$ | $k_l$ | $R^2$ | $n$ | $k_f$ | $R^2$ |
| GnZnO | 78.74016 | 0.37574 | 0.9895 | 3.149606 | 23.47415 | 0.9118 |
| GnZVI | 74.62687 | 0.39528 | 0.9738 | 3.976143 | 26.57577 | 0.8415 |

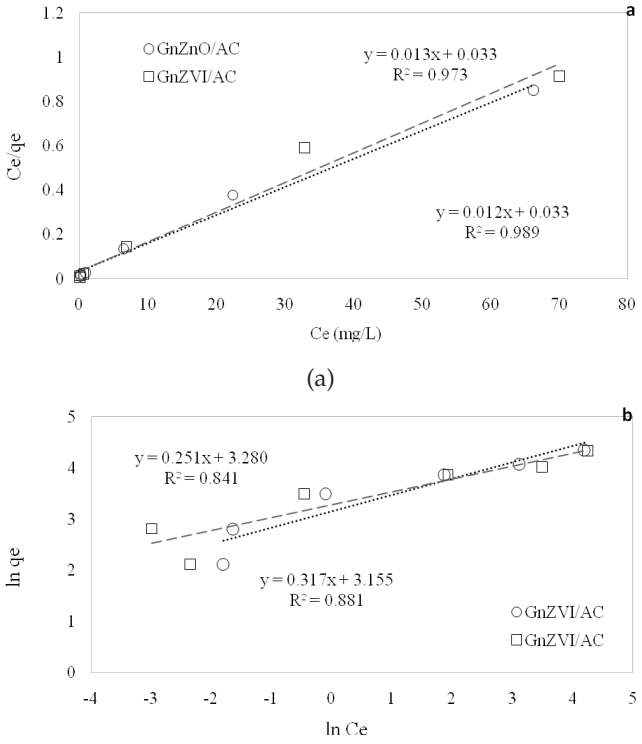


Fig. 8. Langmuir (a), Freundlich (b) plots for MB adsorption on GnZVI/AC and GnZnO/AC.

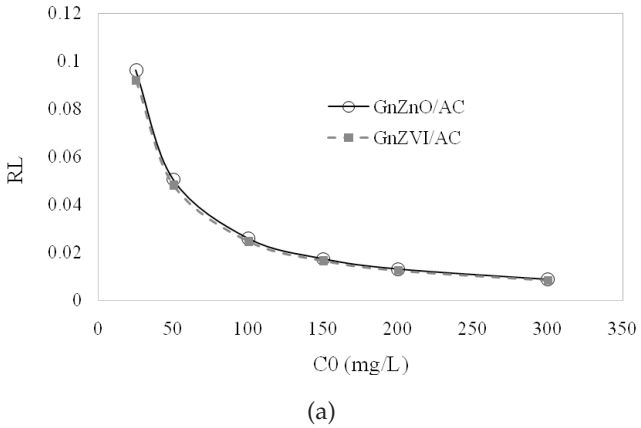


Fig. 9. $R_L$ plots of GnZnO/AC and GnZVI/AC in Langmuir model.

of adsorbent with pollutant, are very important in the formation of adsorption activity [70]. MB adsorption mechanism can be made to the following possible methods:

1. Due to the small size and high specific surface area adsorbents, the removal of MB can occur in monolayer behavior by sedimentation and separation of the adsorbents from solution [41]. The results of the BET analysis indicate a high specific surface of adsorbents, and it can be stated that this mechanism plays a major role in MB removal. The higher specific surface of GZnO/AC is responsible for the higher MB removal efficiency compared to GnZVI/AC .
2. The MB electrostatic adsorption mechanism occurs on GnZnO and GnZVI with pH changes.
   Investigating the effect of pH on MB adsorption showed that increasing pH resulted in an increase in MB adsorption capacity on GnZnO/AC and GnZVI/AC.
   When the pH < pHzpc, the adsorbent surface negatively charged and leads to electrostatic adsorption of cationic MB on the adsorbents surface and the electrostatic adsorption mechanism becomes stronger with increasing pH [70].
3. The role of pores on adsorbents in the removal of Mb can be significant. The BET analysis showed that the pore volume of GnZnO/AC is approximately twice the pore volume of the GnZVI/AC. Therefore, it can be concluded that the higher removal efficiency of GnZnO is due to its greater pore volume compared to the GnZVI [41].

## 4. Conclusions

The results obtained in this study are as follows:

1. *P. harmala* seeds extract could be applied for the synthesis of GnZVI and GnZnO nanoparticles.
2. TEM analysis showed that the size of GnZnO and GnZVI is smaller than 100 nm.
3. EDAX analysis showed that GnZnO and GnZVI were loaded on activated carbon.
4. FTIR showed that polyphenol functional groups had important role in the synthesis and stabilization of nanoparticles. The loading of nanoparticles on AC changed in bonds existing on it.
5. FESEM images showed the loading of nanoparticles on AC. It was observed that there was a more uniform loading of GnZnO as compared with GnZVI located on AC.

Table 3
The comparison of maximum MB adsorption capacities of various adsorbents based on the Langmuir isotherm model

| Adsorbents | pH | Time (min) | Dose (g/l) | $q_{max}$ (mg/g) | Reference |
|---|---|---|---|---|---|
| Seaweed–zinc oxide–polyaniline (SW–ZnO–PANI) | 7 | 10 | 0.5 | 20.55 | [65] |
| Activated carbon nanofibers (ACNFs) | – | 60 | 0.01 | 72.46 | [66] |
| Cork and paper waste-based activated carbon | 11.5 | 5 | 2 | 333.33 | [67] |
| Nano-zerovalent iron | 9.5 | 1 | 0.5 | 208.33 | [68] |
| Banana trunk waste as activated carbon | – | 20 | 1.5 | 166.51 | [69] |
| Reed biochar supported hydroxyapatite nanocomposite | 8 | 600 | 1 | 21.1 | [70] |
| Activated carbon coated with zinc oxide (ZnO) nanoparticles | 11 | 120 | 1.5 | 32.22 | [71] |
| Glycerol based carbon materials | 7 | 120 | 0.02 | 754 | [72] |
| Activated carbon developed from Ficuscaricabast (FCBAC) | 7.8 | 80 | 5 | 47.62 | [73] |
| Walnut shells powder | 6.8 | 40 | 0.5 | 178.9 | [74] |
| A$Fe_3O_4$/activated montmorillonite ($Fe_3O_4$/Mt) nanocomposite | 7.37 | 25 | 0.5 | 106.38 | [75] |
| GnZnO/AC | 11 | 15 | 3 | 78.74 | This work |
| GnZVI/AC | 11 | 40 | 3 | 74.63 | This work |

6. Adsorption analysis showed that by pH, contact time, adsorbent dose, and mixing speed increasing, the adsorption efficiency increased, while increasing initial dye concentration reduced the removal efficiency.
7. The efficiency of MB removal by GnZnO/AC was higher than GnZVI/AC.
8. The laboratory data for both adsorbents follows the second-order kinetic, while the adsorption speed of methylene blue by GnZnO/AC was higher than GnZVI/AC.
9. Adsorption of MB on both adsorbents best fitted with *Langmuir* model as monolayer phase on a homogenous surface. The maximum adsorption capacity of GnZnO/AC and GnZVI/AC for MB were 78.74 and 74.62 mg/g that indicate adsorption capability of GnZnO/AC is higher than GnZVI/AC.
10. The results showed that GnZnO/AC and GnZVI/AC could be effective and appropriate adsorbents to remove methylene blue dye from aquatic solutions.

## Acknowledgment

The author thanks *BirjandUniversity of Medical Sciences* for financial and technical supporting.

## References

[1] M. Qasemi, M. Afsharnia, A. Zarei, M. Farhang, M. Allahdadi, Non-carcinogenic risk assessment to human health due to intake of fluoride in the groundwater in rural areas of Gonabad and Bajestan, Iran: A case study, Human Ecol. Risk Assess., (2018) 1–12.
[2] M. Ghaderpoori, M. Paydar, A. Zarei, H. Alidadi, A.A. Najafpoor, A.H. Gohary, et al., Health risk assessment of fluoride in water distribution network of Mashhad, Iran, Human Ecol. Risk Assess., (2018) 1–12.
[3] M. Fahiminia, A. Paksa, A. Zarei, M. Shams, H. Bakhtiari, M. Norouzi, Survey of optimal methods for the control of cockroaches in sewers of Qom City, Iranian J. Health Environ., 3(1) (2010) 19–26.
[4] M.H. Dehghani, E. Nikfar, A. Zarei, N.M. Esfahani, The effects of US/$H_2O_2$ processes on bisphenol-A toxicity in aqueous solutions using Daphnia magnad, Desal. Water Treat., 68 (2017) 183–189.
[5] K. Elumalai, S. Velmurugan, S. Ravi, V. Kathiravan, G. Adaikala Raj, Bio-approach: Plant mediated synthesis of ZnO nanoparticles and their catalytic reduction of methylene blue and antimicrobial activity, Adv. Powder Technol., 26(6) (2015) 1639–1651.
[6] A.R. Rahmani, A. Shabanloo, M. Fazlzadeh, Y. Poureshgh, H. Rezaeivahidian, Degradation of Acid Blue 113 in aqueous solutions by the electrochemical advanced oxidation in the presence of persulfate, Desal. Water Treat., 59 (2017) 202–209.
[7] A. Seid-Mohammadi, A. Shabanloo, M. Fazlzadeh, Y. Poureshgh, Degradation of acid blue 113 by US/$H_2O_2$/$Fe^{2+}$ and US/$S_2O_8^{2-}$/$Fe^{2+}$ processes from aqueous solutions, Desal. Water Treat., 78 (2017) 273–280.
[8] D. Dutta, S. Chandra, A.K. Swain, D. Bahadur, $SnO_2$ Quantum dots-reduced graphene oxide composite for enzyme-free ultrasensitive electrochemical detection of urea, Anal. Chem., 86(12) (2014) 5914–5921.
[9] M. Rafatullah, O. Sulaiman, R. Hashim, A. Ahmad, Adsorption of methylene blue on low-cost adsorbents: A review, J. Hazard. Mater., 177 (2010) 70–80.
[10] H. Chen, J. Zhao, G. Dai, Silkworm exuviae—A new non-conventional and low-cost adsorbent for removal of methylene blue from aqueous solutions, J. Hazard. Mater., 186(2–3) (2011) 1320–1327.
[11] S. Marković, A. Stanković, Z. Lopičić, S. Lazarević, M. Stojanović, D. Uskoković, Application of raw peach shell particles for removal of methylene blue, J. Environ. Chem. Eng., 3(2) (2015) 716–724.
[12] A.R. Rahmani, A. Shabanloo, M. Fazlzadeh, Y. Poureshgh, Investigation of operational parameters influencing in treatment of dye from water by electro-Fenton process, Desal. Water Treat., 57(51) (2016) 24387–24394.
[13] A. Afkhami, M. Saber-Tehrani, H. Bagheri, Modified maghemite nanoparticles as an efficient adsorbent for removing some cationic dyes from aqueous solution, Desalination, 263 (2010) 240–248.
[14] Z. Zhang, Z. Zhang, Y. Fernández, J.A. Menéndez, H. Niu, J. Peng, L. Zhang, H. Guo, Adsorption isotherms and kinetics of methylene blue on a low-cost adsorbent recovered from a spent catalyst of vinyl acetate synthesis, Appl. Surf. Sci., 256(8) (2010) 2569–2576.

[15] M. Ertas, B. Acemioglu, M. H. Alma, M. Usta, Removal of methylene blue from aqueous solution using cotton stalk, cotton waste and cotton dust, J Hazard Mater. 183 (2010) 421–427.
[16] M. Fazlzadeh, H. Abdoallahzadeh, R. Khosravi, B. Alizadeh, Removal of acid black 1 from aqueous solutions using $Fe_3O_4$ magnetic nanoparticles, J. Mazandaran Univ. Med. Sci., 26(143) (2016) 174–186.
[17] A. Asfaram, M. Ghaedi, S. Hajati, M. Rezaeinejad, A. Goudarzi, M.K. Purkait, Rapid removal of Auramine-O and Methylene blue by ZnS:Cu nanoparticles loaded on activated carbon: A response surface methodology approach, J. Taiwan Inst. Chem. Eng., 53 (2015) 80–91.
[18] Z. Heidarinejad, O. Rahmanian, M. Fazlzadeh, M. Heidari, Enhancement of methylene blue adsorption onto activated carbon prepared from Date Press Cake by low frequency ultrasound, J. Molec. Liq., 264(2018) 591–599.
[19] S. Jain, R.V. Jayaram, Removal of basic dyes from aqueous solution by low-cost adsorbent: Wood apple shell (Feronia acidissima), Desalination, 250(3) (2010) 921–927.
[20] R. Khosravi, M. Fazlzadehdavil, B. Barikbin, H. Hossini, Electro-decolorization of Reactive Red 198 from aqueous solutions using aluminum electrodes systems: modeling and optimization of operating parameters, Desal. Water Treat., 54(11) (2015) 3152–3160.
[21] R. Khosravi, H. Hossini, M. Heidari, M. Fazlzadeh, H. Biglari, A. Taghizadeh, B. Barikbin, Electrochemical decolorization of reactive dye from synthetic wastewater by mono-polar aluminum electrodes system, Int. J. Electrochem. Sci., 12 (2017) 4745–4755.
[22] R. Khosravi, S. Hazrati, M. Fazlzadeh, Decolorization of AR18 dye solution by electrocoagulation: sludge production and electrode loss in different current densities, Desal. Water Treat., 57(31) (2016) 14656–14664.
[23] H. Abdoallahzadeh, B. Alizadeh, R. Khosravi, M. Fazlzadeh, Efficiency of EDTA modified nanoclay in removal of humic acid from aquatic solutions, J. Mazandaran Univ. Med. Sci., 26(139) (2016) 111–125.
[24] A. Dargahi, M. Pirsaheb, S. Hazrati, M. Fazlzadehdavil, R. Khamutian, T. Amirian, Evaluating efficiency of $H_2O_2$ on removal of organic matter from drinking water, Desal. Water Treat., 54(6) (2015) 1589–1593.
[25] E. Azizl, M. Fazlzadeh, M. Ghayebzadeh, L. Hemati, M. Beikmohammadi, H.R. Ghaffari, et al., Application of advanced oxidation process ($H_2O_2$/UV) for removal of organic materials from pharmaceutical industry effluent, Environ. Protect. Eng., 43(1) (2017) 183–191.
[26] R. Khosravi, A. Zarei, M. Heidari, A. Ahmadfazeli, M. Vosughi, M. Fazlzadeh, Application of ZnO and $TiO_2$ nanoparticles coated onto montmorillonite in the presence of $H_2O_2$ for efficient removal of cephalexin from aqueous solutions, Korean J. Chem. Eng., 35(4) (2018) 1000–1008.
[27] S. Norouzi, M. Heidari, V. Alipour, O. Rahmanian, M. Fazlzadeh, F. Mohammadi-moghadam, et al., Preparation, characterization and Cr(VI) adsorption evaluation of NaOH-activated carbon produced from Date Press Cake; an agro-industrial waste, Bioresour. Technol., 258 (2018) 48–56.
[28] M.H. Dehghani, M. Farhang, M. Alimohammadi, M. Afsharnia, G. Mckay, Adsorptive removal of fluoride from water by activated carbon derived from $CaCl_2$-modified Crocus sativus leaves: Equilibrium adsorption isotherms, optimization, and influence of anions, Chem. Eng. Commun., 205(7) (2018) 955–965.
[29] M. Moradi, M. Soltanian, M. Pirsaheb, K. Sharafi, S. Soltanian, A. Mozafari, The efficiency study of pumice powder to lead removal from the aquatic environment: isotherms and kinetics of the reaction, J. Mazandaran Univ. Med. Sci., 23 (2014).
[30] M. Moradi, M. Fazlzadehdavil, M. Pirsaheb, Y. Mansouri, T. Khosravi, K. Sharafi, Response surface methodology (RSM) and its application for optimization of ammonium ions removal from aqueous solutions by pumice as a natural and low cost adsorbent, Archives Environ. Protect., 42(2) (2016) 33–43.
[31] M. Moradi, A.M. Mansouri, N. Azizi, J. Amini, K. Karimi, K. Sharafi, Adsorptive removal of phenol from aqueous solutions by copper (cu)-modified scoria powder: process modeling and kinetic evaluation, Desal. Water Treat., 57(25) (2016) 11820–11834.
[32] D. Naghipour, K. Taghavi, J. Jaafari, Y. Mahdavi, M. Ghanbari Ghozikali, R. Ameri, et al., Statistical modeling and optimization of the phosphorus biosorption by modified Lemna minor from aqueous solution using response surface methodology (RSM), Desal. Water Treat., 57(41) (2016) 19431–19442.
[33] G.H. Safari, M. Zarrabi, M. Hoseini, H. Kamani, J. Jaafari, A.H. Mahvi, Trends of natural and acid-engineered pumice onto phosphorus ions in aquatic environment: adsorbent preparation, characterization, and kinetic and equilibrium modeling, Desal. Water Treat., 54(11) (2015) 3031–3043.
[34] J. Jaafari, M.G. Ghozikali, A. Azari, M.B. Delkhosh, A.B. Javid, A.A. Mohammadi, S. Agarwal, V.K. Gupta, M. Sillanpää, A.G. Tkachev, A.E. Burakov, Adsorption of p-Cresol on $Al_2O_3$ coated multi-walled carbon nanotubes: Response surface methodology and isotherm study, J. Ind. Eng. Chem., 57 (2018) 396–404.
[35] J. Jaafari, K. Yaghmaeian, Optimization of heavy metal biosorption onto freshwater algae (Chlorella coloniales) using response surface methodology (RSM), Chemosphere, 217 (2019) 447–455.
[36] M. Fazlzadeh, R. Khosravi, A. Zarei, Green synthesis of zinc oxide nanoparticles using Peganum harmala seed extract, and loaded on Peganum harmala seed powdered activated carbon as new adsorbent for removal of Cr(VI) from aqueous solution, Ecol. Eng., 103(Part A) (2017) 180–190.
[37] S. Parastar, S. Nasseri, S.H. Borji, M. Fazlzadeh, A.H. Mahvi, A.H. Javadi, M. Gholami, Application of Ag-doped $TiO_2$ nanoparticle prepared by photodeposition method for nitrate photocatalytic removal from aqueous solutions, Desal. Water Treat., 51 (37–39) (2013) 7137–7144.
[38] Q. Sun, H. Li, S. Zheng, Z. Sun, Characterizations of nano-$TiO_2$/diatomite composites and their photocatalytic reduction of aqueous Cr(VI), Appl. Surf. Sci., 311 (2014) 369–376.
[39] R. Khosravi, A. Zarei, M. Fazlzadeh, Investigation of $TiO_2$ and ZnO nanoparticles coated on raw pumice for efficient removal of ethidium bromide from aqueous solutions, Fresenius Environ. Bull., 26(2 A) (2017) 1352–1358.
[40] M. Leili, M. Fazlzadeh, A. Bhatnagar, Green synthesis of nano-zero-valent iron from nettle and thyme leaf extracts and their application for the removal of cephalexin antibiotic from aqueous solutions, Environ. Technol. (UK), 39(9) (2018) 1158–1172.
[41] M. Fazlzadeh, K. Rahmani, A. Zarei, H. Abdoallahzadeh, F. Nasiri, R. Khosravi, A novel green synthesis of zero valent iron nanoparticles (NZVI) using three plant extracts and their efficient application for removal of Cr (VI) from aqueous solutions, Adv. Powder Technol., 28(1) (2017) 122–130.
[42] A. Gholami, R. Khosravi, A. Khosravi, Z. Samadi, Data on the optimization of the synthesis of green iron nanoparticles using plants indigenous to South Khorasan, Data in Brief, 21 (2018) 1779–1783.
[43] M. Fazlzadeh, M. Ansarizadeh, M. Leili, Data of furfural adsorption on nano zero valent iron (NZVI) synthesized from Nettle extract, Data in Brief, 16 (2018) 341–345.
[44] A. Astulla, K. Zaima, Y. Matsuno, Y. Hirasawa, W. Ekasari, A. Widyawaruyanti, N.C. Zaini, H. Morita, Alkaloids from the seeds of Peganum harmala showing antiplasmodial and vasorelaxant activities, J. Nat. Med., 62(4) (2008) 470–472.
[45] A.M. Sobhani, S.-A. Ebrahimi, M. Mahmoudian, An in vitro evaluation of human DNA topoisomerase I inhibition by Peganum harmala L. seeds extract and its beta-carboline alkaloids, J. Pharm. Pharm. Sci., 5(1) (2002) 19–23.
[46] G. Moussavi, R. Khosravi, The removal of cationic dyes from aqueous solutions by adsorption onto pistachio hull waste, Chem. Eng. Res. Design, 89(10) (2011) 2182–2189.
[47] A.A. Najafpoor, A. Sadeghi, H. Alidadi, M. Davoudi, B. Mohebrad, A. Hosseinzadeh, S. Jafarpour, A. Zarei, Biodegradation of high concentrations of phenol by baker's yeast in anaerobic sequencing batch reactor, Environ. Health Eng. Manage. J., 2(2) (2015) 79–86.

[48] M. Ghaedi, A.G. Nasab, S. Khodadoust, R. Sahraei, A. Daneshfar, Characterization of zinc oxide nanorods loaded on activated carbon as cheap and efficient adsorbent for removal of methylene blue, J. Ind. Eng. Chem., 21 (2015) 986–993.
[49] V. Madhavi, T.N. Prasad, A.V. Reddy, B. Ravindra Reddy, G. Madhavi, Application of phytogenic zerovalent iron nanoparticles in the adsorption of hexavalent chromium, Spectrochim. Acta Part A, Molec.Biomolec. Spectroscopy, 116 (2013) 17–25.
[50] L. Huang, X. Weng, Z. Chen, M. Megharaj, R. Naidu, Synthesis of iron-based nanoparticles using oolong tea extract for the degradation of malachite green, Spectrochim. Acta Part A, Molec. Biomolec. Spectroscopy, 117 (2014) 801–804.
[51] G. Sangeetha, S. Rajeshwari, R. Venckatesh, Green synthesis of zinc oxide nanoparticles by aloe barbadensis miller leaf extract: Structure and optical properties, Mater. Res. Bull., 46(12) (2011) 2560–2566.
[52] A. Ray, S.D. Gupta, S. Ghosh, Evaluation of anti-oxidative activity and UV absorption potential of the extracts of Aloe vera L. gel from different growth periods of plants, Ind. Crops Products, 49 (2013) 712–719.
[53] K.S. Prasad, P. Gandhi, K. Selvaraj, Synthesis of green nano iron particles (GnIP) and their application in adsorptive removal of As(III) and As(V) from aqueous solution, Appl. Surf. Sci., 317 (2014) 1052–1059.
[54] A. Bhatnagar, Removal of bromophenols from water using industrial wastes as low cost adsorbents, J. Hazard. Mater., 139 (2007) 93–102.
[55] N. Nasuha, B.H. Hameed, A.T.M. Din, Rejected tea as a potential low-cost adsorbent for the removal of methylene blue, J. Hazard. Mater., 175 (2010) 126–132.
[56] Z. Noorimotlagh, R.D.C. Soltani, G.S. Khorramabadi, H. Godini, M. Almasian,Performance of wastewater sludge modified with zinc oxide nanoparticles in the removal of methylene blue from aqueous solutions, Desal. Water Treat., 57(4) (2016) 1684–1692.
[57] A. A. Alqadami, M. Naushad, M.A. Abdalla, M.R. Khan, Z.A. Alothman, Adsorptive removal of toxic dye using $Fe_3O_4$–TSC nanocomposite: equilibrium, kinetic, and thermodynamic studies, J. Chem. Eng. Data, 61(11) (2016) 3806–3813.
[58] A.A. Alqadami, M. Naushad, Z.A. Alothman, A.A. Ghfar, Novel metal–organic framework (MOF) based composite material for the sequestration of U (VI) and Th (IV) metal ions from aqueous environment, ACS Appl. Mater. Interf., 9(41) (2017) 36026–36037.
[59] A.E. Yilmaz, R. Boncukcuoğlu, M. Kocakerim, İ.H. Karakaş, Waste utilization: The removal of textile dye (Bomaplex Red CR-L) from aqueous solution on sludge waste from electrocoagulation as adsorbent, Desalination, 277 (2011) 156–163.
[60] Ö. Gerçel, H.F. Gerçel, A.S. Koparal, Ü.B. Öğütveren, Removal of disperse dye from aqueous solution by novel adsorbent prepared from biomass plant material, J. Hazard. Mater., 160 (2008) 668–674.
[61] B.H. Hameed, R.R. Krishni, S.A. Sata, A novel agricultural waste adsorbent for the removal of cationic dye from aqueous solutions, J. Hazard. Mater., 162 (2009) 305–311.
[62] M. Qasemi, M. Afsharnia, A. Zarei, A.A. Najafpoor, S. Salari, M. Shams, Phenol removal from aqueous solution using Citrullus colocynthis waste ash, Data in Brief, 18 (2018) 620–628.
[63] M. Ghaedi, M. Ghayedi, S.N. Kokhdan, R. Sahraei, A. Daneshfar, Palladium, silver, and zinc oxide nanoparticles loaded on activated carbon as adsorbent for removal of bromophenol red from aqueous solution, J. Ind. Eng. Chem., 19(4) (2013) 1209–1217.
[64] K.S. Prasad, P. Gandhi, K. Selvaraj, Synthesis of green nano iron particles (GnIP) and their application in adsorptive removal of As (III) and As (V) from aqueous solution, Appl. Surf. Sci., 317 (2014) 1052–1059.
[65] R. Pandimurugan, S. Thambidurai, Synthesis of seaweed-ZnO-PANI hybrid composite for adsorption of methylene blue dye, J. Environ. Chem. Eng., 4(1) (2016) 1332–1347.
[66] A.S. Ibupoto, U.A. Qureshi, F. Ahmed, Z. Khatri, M. Khatri, M. Maqsood, R.Z. Brohi, I.S. Kim, Reusable carbon nanofibers for efficient removal of methylene blue from aqueous solution, Chem. Eng. Res. Design, 136 (2018) 744–752.
[67] R.M. Novais, A.P. Caetano, M.P. Seabra, J.A. Labrincha, R.C. Pullar, Extremely fast and efficient methylene blue adsorption using eco-friendly cork and paper waste-based activated carbon adsorbents, J. Cleaner Prod., 197 (2018) 1137–1147.
[68] S. Arabi, M.R. Sohrabi, Removal of methylene blue, a basic dye, from aqueous solutions using nano-zerovalent iron, Water Sci. Technol., 70(1) (2014) 24–31.
[69] M. Danish, T. Ahmad, S. Majeed, M. Ahmad, L. Ziyang, Z. Pin, S.M. Shakeel Iqubal, Use of banana trunk waste as activated carbon in scavenging methylene blue dye: kinetic, thermodynamic, and isotherm studies, Bioresou. Technol. Reports, 3 (2018) 127–137.
[70] Y. Li, Y. Zhang, G. Wang, S. Li, R. Han, W. Wei, Reed biochar supported hydroxyapatite nanocomposite: Characterization and reactivity for methylene blue removal from aqueous media, J. Molec. Liq., 263 (2018) 53–63.
[71] H. Nourmoradi, A. Ghiasvand, Z. Noorimotlagh, Removal of methylene blue and acid orange 7 from aqueous solutions by activated carbon coated with zinc oxide (ZnO) nanoparticles: equilibrium, kinetic, and thermodynamic study, Desal. Water Treat., 55 (2015) 252–262.
[72] A.A. Narvekar, J. Fernandes, S. Tilve, Adsorption behavior of methylene blue on glycerol based carbon materials, J. Environ. Chem. Eng., 6(2) (2018) 1714–1725.
[73] D. Pathania, S. Sharma, P. Singh, Removal of methylene blue by adsorption onto activated carbon developed from Ficus carica bast, Arabian J. Chem., 10 (2017) S1445–S1451.
[74] Y. Miyah, A. Lahrichi, M. Idrissi, A. Khalil, F. Zerrouq, Adsorption of methylene blue dye from aqueous solutions onto walnut shells powder: Equilibrium and kinetic studies, Surfaces Interfaces, 11 (2018) 74–81.
[75] J. Chang, J. Ma, Q. Ma, D. Zhang, N. Qiao, M. Hu, H. Ma, Adsorption of methylene blue onto $Fe_3O_4$/activated montmorillonite nanocomposite, Appl. Clay Sci., 119 (2016) 132–140.